Available online at www.sciencedirect.com
ScienceDirect
Trans. Nonferrous Met. Soc. China 33(2023) 201−208
Transactions of Nonferrous Metals Society of China
www.tnmsc.cn

Microstructure characterization of $(Sn_{1-x}Zn_x)_{57}(In_{0.78}Bi_{0.22})_{43}$ low melting point lead-free solder materials

Tian-yu ZHANG, Qing CHENG, Heng-yu ZHU, Qin-qin WEI, Xian-dong XU

Centre for High Resolution Electron Microscopy, College of Materials Science and Engineering, Hunan University, Changsha 410082, China

Received 13 October 2021; accepted 12 January 2022

Abstract: $(Sn_{1-x}Zn_x)_{57}(In_{0.78}Bi_{0.22})_{43}$ (x=0.10, 0.15, 0.20, at.%) quaternary alloys were designed and characterized based on the multi-principal-element mixing concept in order to develop a lead-free solder suitable for low temperature soldering in three-dimensional integrated circuit. The microstructure, thermal properties and wetting properties of the alloys were investigated using scanning electron microscope, X-ray diffractometer and differential scanning calorimeter. The results show that the alloys consist of intermetallic compounds (IMCs), $BiIn_2$ and $In_{0.2}Sn_{0.8}$, and Zn-rich solid solution. With the increase of Zn content, the volume fractions of the $BiIn_2$ and Zn-rich phases increase accordingly. The alloys exhibit low melting points of about 70 °C, due to the formation of the low-melting-point $In_{0.2}Sn_{0.8}$ and $BiIn_2$ IMCs. The alloys show good wetting properties with wetting angle of about 40°. At the solder joints between the alloys and Cu layer, a thin and tough Cu_5Zn_8 layer is formed, which is supposed to improve the joint reliability. It is demonstrated that the welding performance of solders can be effectively enhanced by designing solders through the multi-principal-element mixing concept.

Key words: lead-free solder; multi-principal-element mixing; low melting point; microstructure; thermal properties

1 Introduction

According to the Moore's law, the component in semiconductor industry is approaching its size limit [1−3]. Those semiconductor components are not be able to meet the requirement for performance and cost of manufacturing integrated circuits. The most promising way to break through the bottleneck encountered in the electronic packaging industry is to develop from a two-dimensional integrated circuit (2D integrated circuit, 2D-IC) to a three-dimensional integrated circuit (3D integrated circuit, 3D-IC) [4−6]. TSV (through silicon via) technology used in 3D-IC can vertically stack multi-layer silicon chips through micro-bumps (μ-Bumps) to reduce the interconnection length and then achieve low power consumption, high speed, and miniaturization [7−9]. Two key problems affect the application of 3D-IC. The first one is the silicon wafer warpage, which is caused by the mismatch of the thermal expansion coefficient as the thickness of the silicon wafer in the 3D-IC is reduced from 200 to 50 μm [10,11]. The other problem is the reliability of solder joints caused by the excessive brittle IMCs [12−14]. Therefore, the research and development of novel solder materials with low melting point, low IMCs growth rate and good wettability has gained extensive attention.

The most common binary eutectic solders in the field of low temperature soldering are Sn−Zn solder, Sn−Bi solder and Sn−In solder [15−18]. Their melting points are above 100 °C, and the wettability, mechanical properties and economics

Corresponding author: Xian-dong XU, Tel: +86-15616213618, E-mail: xiandongxu@hnu.edu.cn;
Qin-qin WEI, Tel: +86-18973197475, E-mail: weiqq2017@126.com
DOI: 10.1016/S1003-6326(22)66100-4

cannot be well unified. Compositional design aided by the multi-principal-element mixing has been reported to be effective in improving the performance of solders [19−21]. For instance, it has been found that addition of 1 wt.% In to $Zn_{30}Sn$ to replace Zn reduces the melting point of the solder by 29.6 °C [22]. The In element added does not promote the formation of new IMCs, but dissolves in the Sn-rich phase to form β-Sn with a lower melting point. Similarly, the addition of 2 wt.% In to a Sn−Bi lead-free solder was demonstrated to further decrease the melting point by 10 °C, which is caused by the formation of $InSn_{19}$ intermetallic compounds [23]. Nevertheless, the addition of a small amount of low melting point elements to further reduce the melting point of the solder does not meet the requirements of the modern electronic packaging industry.

A ternary low-temperature solder In−32.7Bi−0.5Zn (In−Bi−Zn) with a melting point of only 72 °C was reported [24]. However, due to the high cost of the main component In metal, the application of the solder is limited. Recently, it has been demonstrated that in an equi-atomic high-entropy alloy (HEA) consisting of Zn, Bi, In, and Zn, the melting point of the solder could be further lowered to about 80 °C, and the wetting angle was about 52 °C [25]. However, the precipitation of brittle Bi phase in the HEA may deteriorate mechanical and welding properties.

In this work, based on the binary eutectic phase diagrams of three common low-temperature solders, Sn−Bi, Bi−In, and Sn−Zn, combined with the eutectic point composition in the eutectic phase diagram, a new type of $(Sn_{1-x}Zn_x)_{57}(In_{0.78}Bi_{0.22})_{43}$ (x=0.10, 0.15, 0.20, at.%) quaternary low melting point solder was designed, aided by the multi-principal-element mixing concept, providing an alternative new solder for 3D-IC manufacturing. The synergic elemental interactions and the resultant microstructures were carefully investigated to correlate with the low melting characteristics observed for the alloy.

2 Experimental

Ingots with a nominal composition of $(Sn_{1-x}Zn_x)_{57}(In_{0.78}Bi_{0.22})_{43}$ (x=0.10, 0.15, 0.20, at.% Table 1) were prepared with high purity elements (larger than 99.99%) by induction melting and conventional casting (model IMCS−2000−E) under a high-purity argon atmosphere. A slight positive pressure (0.04 MPa) was kept to minimize the elemental evaporation. The ingots were remelted three times to ensure chemical homogeneity. To characterize melting characteristics of the solder alloy, a synchronous differential scanning calorimetry (DSC, STA449F5) was used to test the heat flow with a gas flow rate of 50 mL/min, temperature range of 30−150 °C and sample mass of 20−30 mg.

Table 1 Nominal chemical compositions of $(Sn_{1-x}Zn_x)_{57}$-$(In_{0.78}Bi_{0.22})_{43}$ solder alloys (at.%)

x	Sn	Zn	In	Bi
0.10	51.30	5.70	33.54	9.46
0.15	48.45	8.55	33.54	9.46
0.20	45.60	11.40	33.54	9.46

Crystal structure analysis of the solder alloys was carried out using an X-ray diffractometer (XRD) with a Cu target. The step length and scanning rate was 0.02 and 4 (°)/min, respectively. Microstructure analysis was performed using an environmental scanning electron microscope (SEM, Quanta 200) equipped with an X-ray energy spectrometer (EDX). A copper sheet with a dimension of 10 mm × 10 mm × 1 mm was utilized to analyze the wetting performance of the solder alloys. To remove the surface oxide, the copper sheet was mechanically polished using 1200#, 2000# and 5000# sandpapers and then placed in an ethanol for ultrasonic cleaning. 0.02 mL of N8860 type flux was taken and dropped on a copper sheet to make the test piece. Then, the test piece was placed on a heating plate, heated at 160 °C for 10 min, and cooled to room temperature. The wetting angle was directly measured from images taken by SEM.

3 Results and discussion

3.1 Microstructure

Figure 1 displays the XRD patterns of $(Sn_{1-x}Zn_x)_{57}(In_{0.78}Bi_{0.22})_{43}$ alloys. The major phase is identified as $In_{0.2}Sn_{0.8}$ by combining XRD and spectrometric EDX analysis (Table 2). Similarly, two other minor phases, namely $BiIn_2$ and Zn IMC phases, are also detected. Obviously, in the XRD pattern of the Bi−Sn−In−Zn solder, no visible peaks

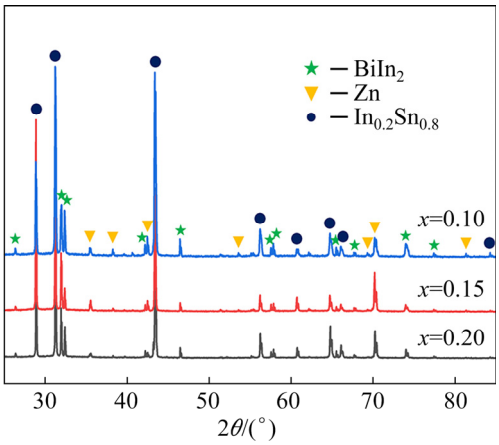

Fig. 1 XRD patterns of $(Sn_{1-x}Zn_x)_{57}(In_{0.78}Bi_{0.22})_{43}$ solder alloys

of Sn and Bi are detected. The low-melting-point metallic element In in the Sn−Bi alloy system is added to form two low-melting-point IMCs, $In_{0.2}Sn_{0.8}$ and $BiIn_2$, with Sn and Bi in the alloy. It is worth noting that Zn does not react with any constituent of the Bi−Sn−In−Zn solder to form IMCs containing Zn [26,27]. This is because of the hexagonal close-packed structure of Zn and its atomic radius of 134 pm, very unlike the other solder constituents [28].

Figure 2 shows backscattered electron (BSE) images of $(Sn_{1-x}Zn_x)_{57}(In_{0.78}Bi_{0.22})_{43}$ alloys. Three different morphologies are identified in all samples from the difference in their contrast. Combined with the corresponding elemental distributions of Bi, In,

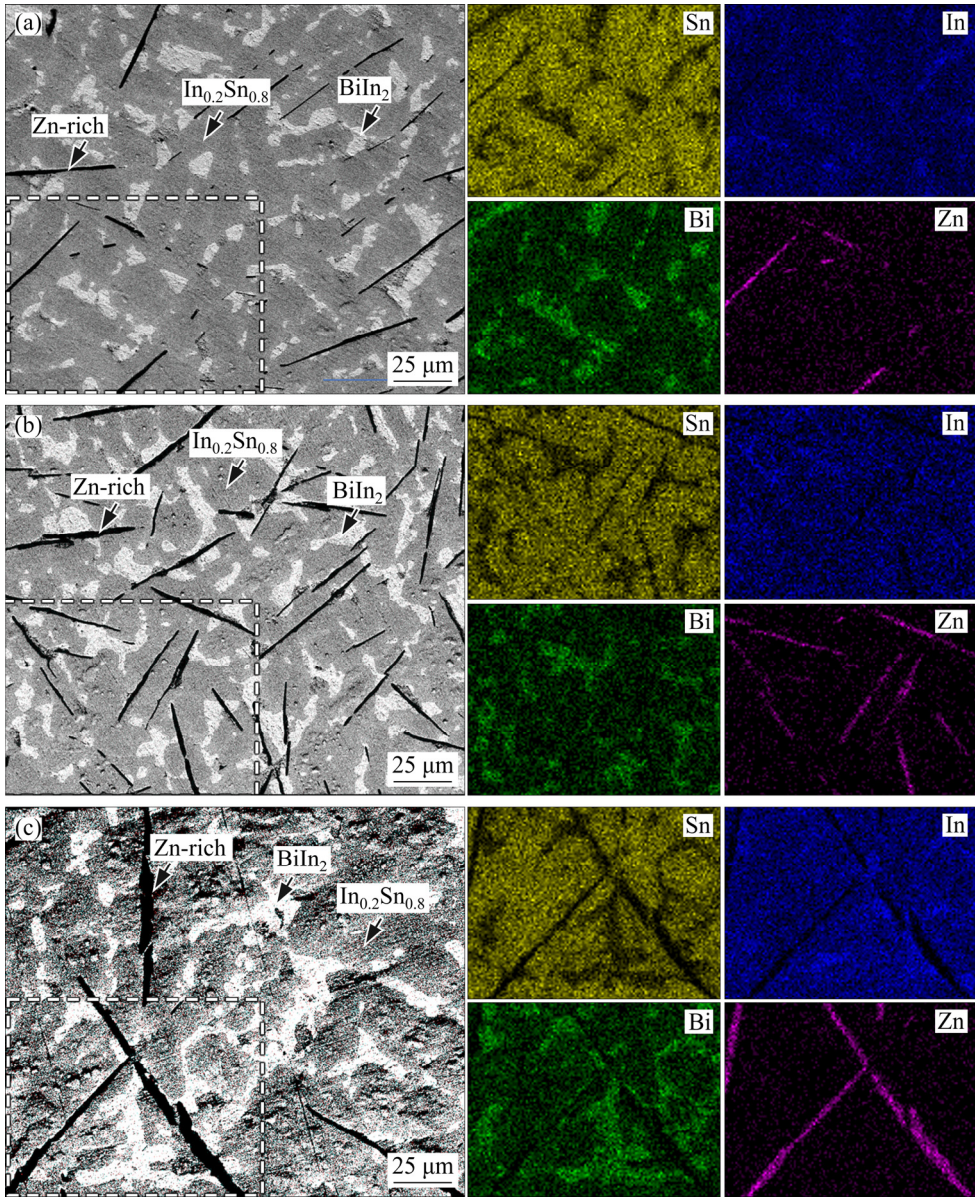

Fig. 2 SEM−BSE images and corresponding EDS mapping of $(Sn_{1-x}Zn_x)_{57}(In_{0.78}Bi_{0.22})_{43}$ solder alloys: (a) x=0.10; (b) x=0.15; (c) x=0.20

Table 2 Measured chemical compositions of phases in $(Sn_{1-x}Zn_x)_{57}(In_{0.78}Bi_{0.22})_{43}$ solder alloys (at.%)

Alloy	Element	$In_{0.2}Sn_{0.8}$	$BiIn_2$	Zn-rich
x=0.10	Sn	57.4±0.6	5.3±0.5	3.8±0.7
	Bi	7.7±0.2	27.6±0.3	1.0±0.2
	In	33.6±0.4	65.5±0.5	3.0±1.8
	Zn	1.3±0.3	1.6±0.5	92.2±2.7
x=0.15	Sn	62.0±5.7	5.5±0.5	4.6±1.5
	Bi	5.9±1.3	27.6±0.1	0.5±0.2
	In	29.9±3.5	64.9±0.6	4.5±0.8
	Zn	2.2±1	2.0±0.9	90.4±2.4
x=0.20	Sn	59.0±1.8	5.6±0.6	4.1±1.1
	Bi	6.8±0.6	27.9±0.1	0.7±0.5
	In	32.6±1.3	64.8±0.5	5.0±1.2
	Zn	1.6±0.2	1.7±0.4	90.2±5.0

Sn and Zn determined by SEM−EDX mappings, the needle-like regions in black are Zn-rich phases, the grey regions are $In_{0.2}Sn_{0.8}$ phases and white regions are $BiIn_2$ phases. The Zn-rich phase exhibits needle-like morphologies and is precipitated along particular crystallographic directions. The observation of needle-like Zn-rich phase is consistent with that observed in the eutectic Sn−9Zn alloy [29,30]. In contrast, the $BiIn_2$ and $In_{0.2}Sn_{0.8}$ phases interpenetrate and connect to form a network. This three-phase coexisting microstructure is similar to that of Sn−45Bi−2.6Zn and $Bi_{53}Sn_{26}Cd$, both of which are composed of two interpenetrating acicular Zn-rich phases [31,32]. It is worth noting that the single phase of Sn and the single phase of Bi are not found in the microstructure of the solder, which improves the reliability of the solder joints because Sn whiskers are easily formed in the pure Sn phase and cause short circuits. The pure Bi phase is brittle and prone to dendrite segregation and coarse structure during solidification. In these alloys, the precipitation of $BiIn_2$ IMCs and Zr-rich phase increases with the increase of Zn content. The chemical compositions of phases were further obtained by EDX analysis. As shown in Table 2, Zn is not detectable with the $BiIn_2$ and $In_{0.2}Sn_{0.8}$ IMCs, supporting the limited solubility of Zn in matrix and as a result, the precipitation of excessive Zn from the matrix can be well explained by the binary phase diagram [30], in which the Zn-rich phase is a solid solution containing small amount of low-melting-point elements.

3.2 Thermal properties and phase formation of Sn−Bi−In−Zn alloys

For the soldering materials, the melting temperature is a key characteristic of low temperature solder. The heating DSC curves of the $(Sn_{1-x}Zn_x)_{57}(In_{0.78}Bi_{0.22})_{43}$ alloys are shown in Fig. 3. Three distinctive endothermic peaks are detected, which correspond to the three phases in the alloys. The melting temperatures of the $In_{0.2}Sn_{0.8}$, $BiIn_2$ and Zn-rich phases were identified to be 59.3, 69.7 and 134.0 °C, respectively. Increasing the Zn addition, the melting temperatures of the $BiIn_2$ and $In_{0.2}Sn_{0.8}$ IMCs change slightly owing to the limited solubility of Zn. The melting temperature of Zn-rich phase changes due to solid solution of low-melting-point elements (Table 2).

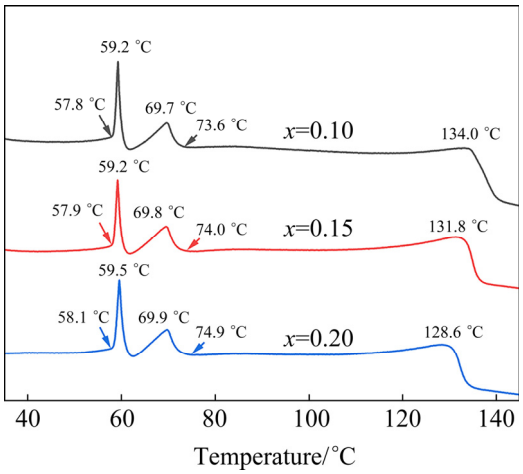

Fig. 3 DSC curves of $(Sn_{1-x}Zn_x)_{57}(In_{0.78}Bi_{0.22})_{43}$ solder alloys

For the solidification process, the Zn-rich phase is supposed to precipitate first due to the highest melting temperature of Zn among the constituent elements in the alloys and limited solubility of Zn. Then, the $BiIn_2$ IMCs precipitate owing to their higher melting temperature than the $In_{0.2}Sn_{0.8}$ IMCs (Fig. 3). Meanwhile, the $BiIn_2$ IMCs are easier to form than other Bi−In IMCs based on the Bi−In binary phase diagram [33]. According to the following equation, the excessive In (Bi) in the alloy reacts with Sn to form the $In_{0.2}Sn_{0.8}$ IMCs with low melting temperature:

$$Bi+In \rightarrow BiIn_2+In(Bi) \quad (1)$$

From the DSC results, the solder matrix $In_{0.2}Sn_{0.8}$ IMCs begin to melt at about 60 °C, and $BiIn_2$ IMCs melt at about 70 °C, indicating low-melting-point of the solder alloys and a certain flow ability. A small amount of Zn-rich phase precipitating in the matrix during the melting process has little effect on the performance of the solder.

3.3 Wettability of Sn−Bi−In−Zn alloy

Wetting angles were measured by placing the solder materials on a Cu sheet and heating up to a target temperature. It is widely accepted that the solder with a small wetting angle has better wetting performance during the soldering process. Therefore, a low-melting-point solder alloy with good properties requires good wetting properties at low temperatures. Figure 4 shows that when soldering at 160 °C, the wetting angle of the quaternary Sn−Bi−In−Zn alloy is very small, showing good wetting performance (compared to other Zn-containing solders). Owing to good wettability, the solder joints can fully contact the substrate, ensure the designed strength of solder joints, and reduce the occurrence of spots. Interestingly, the increase in the Zn content can slightly increase the wettability of the solder on the Cu board, which is slightly different from what we expected. The common Sn−Zn solder exhibits poor oxidation resistance because of high activity of Zn [34]. This results in a higher surface tension of the solder in the liquid state during the soldering process. The following formula shows the relationship between the wetting angle θ and γ_{LF} [35]:

$$\cos\theta = \frac{\gamma_{SF} - \gamma_{LS}}{\gamma_{LF}} \tag{2}$$

where θ represents the wetting angle; γ_{LF}, γ_{SF} and γ_{LS} represent the surface tensions of liquid solder/flux, substrate/flux and liquid solder/substrate, respectively. Under the condition of wetting, the surface tension of liquid solder/flux is proportional to the wetting angle θ. In the present work, as the value of x increases (the Zn content increases), the wetting angle θ of the solder with x=0.15 and x=0.20 composition is slightly lower than that of the solder with x=0.10 composition. However, it does not decrease monotonously with the increase of Zn content in solder [36].

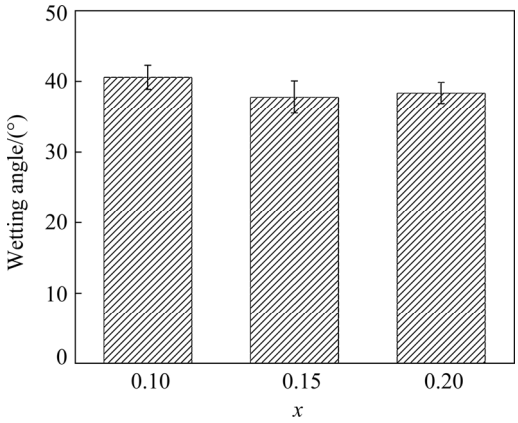

Fig. 4 Wetting angle of $(Sn_{1-x}Zn_x)_{57}(In_{0.78}Bi_{0.22})_{43}$ solder alloys

As a result, the change in the Zn content is supposed to change the composition of the entire quaternary system, which reduces the surface tension of the liquid solder, thereby reducing its wetting angle; on the other hand, although it is not a surface-active element, when reacting with Cu, Zn has larger diffusivity than Sn, Bi and In. As the Zn content in Sn−Bi−In−Zn alloy increases, a lot of Zn atoms diffuse into the Cu substrate to form Cu−Zn IMCs, and the depth of IMCs is about 5 μm, as shown in Fig. 5. This difference in diffusivity breaks the static balance of the solder/copper interface [37] and ensures the soldering edge to extend outward, thereby improving the wettability of the solder on the Cu substrate. It is worth noting that in the quaternary system, after adding Zn, a uniform, thin, and tough Cu_5Zn_8 (IMCs) layer is formed and the thick and brittle Cu_6Sn_5 is completely suppressed [38]. In addition, since the compressive stress generated by Cu_6Sn_5 in the pure Sn phase is the main reason for the formation of whiskers, the solder has a safety hazard. On the contrary, the formation of Cu_5Zn_8 IMCs can avoid this problem and improve the reliability of solder joints.

4 Conclusions

(1) The melting point of the solder is about 70 °C, and the wetting angle during the soldering process is about 40°, which possesses good wetting properties that are suitable as a soldering material for 3D-IC.

(2) The $(Sn_{1-x}Zn_x)_{57}(In_{0.78}Bi_{0.22})_{43}$ alloys consist of three phases, $BiIn_2$ IMCs, $In_{0.2}Sn_{0.8}$ IMCs and

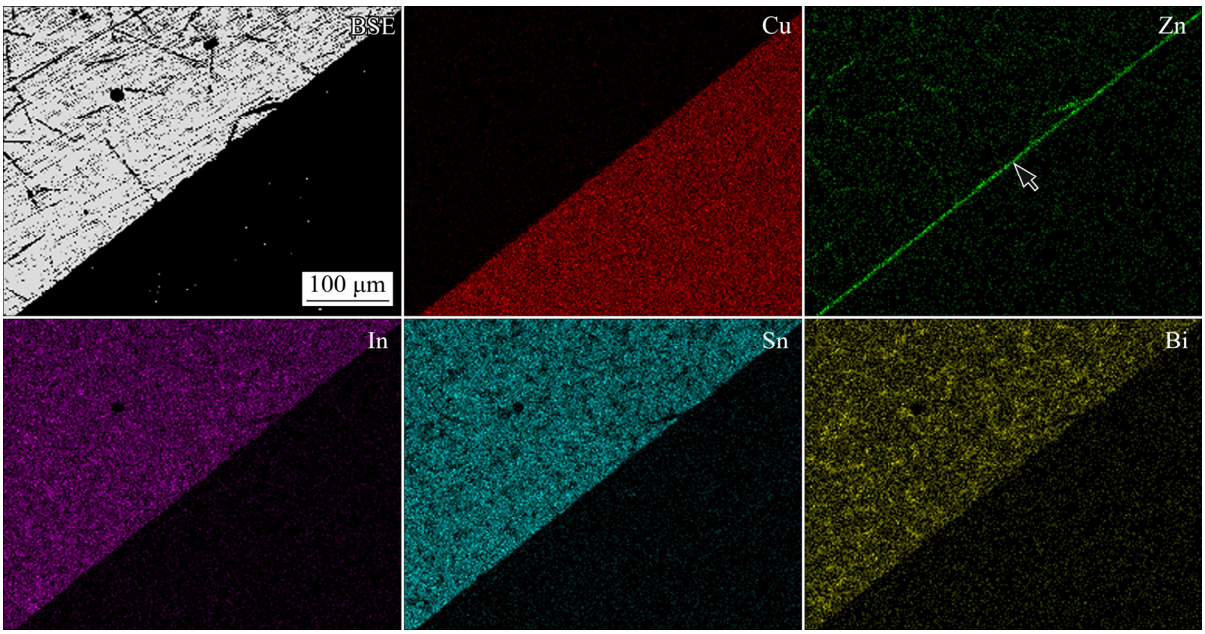

Fig. 5 SEM-BSE image and corresponding EDX mapping of $(Sn_{0.85}Zn_{0.5})_{57}(In_{0.78}Bi_{0.22})_{43}$ solder alloy

Zn-rich solid solution. With the increase of Zn content, the volume fraction of $BiIn_2$ and Zn-rich phases increases accordingly.

(3) The solders possess low melting point owing to the formation of the low-melting-point $In_{0.2}Sn_{0.8}$ (~60 °C) and $BiIn_2$ (~70 °C) phases. The wetting angle of the $(Sn_{1-x}Zn_x)_{57}(In_{0.78}Bi_{0.22})_{43}$ alloys is measured to be 40°. The solders exhibit good wetting properties and are suitable as a soldering material for 3D-IC.

(4) A thin and tough Cu_5Zn_8 IMCs layer is formed between the solder and Cu layer owing to the synergy between multiple elements, improving the welting performance of the solders and the reliability of solder joints.

Acknowledgments

This work was financially supported by the National Natural Science Foundation of China (No. 52001120), the Fundamental Research Funds for the Central Universities, China (No. 531118010450), and the Hundred Talent Program of Hunan Province, China (No. 2021-Z09). One of the authors, Qin-qin WEI, was supported by the Postdoctoral Science Foundation of China (No. 2021M701135) and the Excellent Postdoctoral Innovative Talents Program of Hunan Province, China (No. 2021RC2043). The authors would like to thank Dr. Ying-xia LIU for helpful discussion.

References

[1] LIU Ying-xia, CHU Y C, TU K N. Scaling effect of interfacial reaction on intermetallic compound formation in Sn/Cu pillar down to 1μm diameter [J]. Acta Materialia, 2016, 117: 146−152.

[2] TU K N, LIU Ying-xia, LI Meng-lu. Effect of Joule heating and current crowding on electromigration in mobile technology [J]. Applied Physics Reviews, 2017, 4(1): 011101.

[3] KOBAYASHI M. More than more [J]. The Journal of The Institute of Image Information and Television Engineers, 2016, 70(3): 324−327.

[4] ANNUAR S, MAHMOODIAN R, HAMDI M, TU K N. Intermetallic compounds in 3D integrated circuits technology: A brief review [J]. Science & Technology of Advanced Materials, 2017, 18(1): 693−703.

[5] LIU Ying-xia, TAMURA N, KIM D W, GU S, TU K N. A metastable phase of tin in 3D integrated circuit solder microbumps [J]. Scripta Materialia, 2015, 102: 39−42.

[6] ZHANG Liang, LIU Zhi-quan. Inhibition of intermetallic compounds growth at Sn−58Bi/Cu interface bearing CuZnAl memory particles (2−6 μm) [J]. Journal of Materials Science: Materials in Electronics, 2020, 31(1): 2466−2480.

[7] KOYANAGI M, FUKUSHIMA T, TANAKA T. High-density through silicon vias for 3-D LSIs [J]. Proceedings of the IEEE, 2009, 97(1): 49−59.

[8] SHEN Wen-wei, CHEN Kuan-neng. Three-dimensional integrated circuit (3D IC) key technology: Through-silicon via (TSV) [J]. Nanoscale Research Letters, 2017, 12(1): 56.

[9] WONG C S, BENNETT N S, MANESSIS D, DANILEWSKY A, MCNALLY P J. Non-destructive laboratory-based X-ray diffraction mapping of warpage in Si

die embedded in IC packages [J]. Microelectronic Engineering, 2014, 117: 48−56.

[10] KIM E K. Assessment of ultra-thin Si wafer thickness in 3D wafer stacking [J]. Microelectronics Reliability, 2010, 50(2): 195−198.

[11] LIU C M, LIN Han-wen, HUANG Yi-sa, CHU Yi-cheng, CHEN C, LYU D R, CHEN Kuan-neng, TU K N. Low-temperature direct copper-to-copper bonding enabled by creep on (111) surfaces of nanotwinned Cu [J]. Scientific Reports, 2015, 5: 9734.

[12] CHEN Wei-yu, TU Wei, HSIANG C C, CHOU T T, DUH J G. Growth orientation of Cu−Sn IMC in Cu/Sn−3.5Ag/Cu−*x*Zn microbumps and Zn-doped solder joints [J]. Materials Letters, 2014, 134: 184−186.

[13] HSU H H, HUANG Yi-ting, HUANG Shi-yi, CHANG Tao-chang, WU T C. Evolution of the intermetallic compounds in Ni/Sn−2.5Ag/Ni microbumps for three-dimensional integrated circuits [J]. Journal of Electronic Materials, 2015, 44(10): 3888−3895.

[14] TALEBANPOUR B, HUANG Zhe, CHEN Zhe, DUTTA I. Effect of joint scale and processing on the fracture of Sn−3Ag−0.5Cu solder joints: Application to micro-bumps in 3D packages [J]. Journal of Electronic Materials, 2016, 45(1): 57−68.

[15] SUGANUMA K, KIM K S. Sn−Zn low temperature solder [J]. Journal of Materials Science: Materials in Electronics, 2007, 18(1/2/3): 121−127

[16] CHEN C H, LEE B H, CHEN H C, WANG C M, WU T C. Interfacial reactions of low-melting Sn−Bi−Ga solder alloy on Cu substrate [J]. Journal of Electronic Materials, 2016, 45(1): 197−202.

[17] SILVA B L, REINHART G, NGUYEN-THI H, MANGELINCK-NOËL N, GARCIA A, SPINELLI J E. Microstructural development and mechanical properties of a near-eutectic directionally solidified Sn−Bi solder alloy [J]. Materials Characterization, 2015, 107: 43−53.

[18] TIAN Fei-fei, LIU Zhi-quan, SHANG Pan-ju, GUO Jing-dong. Phase identification on the intermetallic compound formed between eutectic SnIn solder and single crystalline Cu substrate [J]. Journal of Alloys & Compounds, 2014, 591: 351−355.

[19] TUNTHAWIROON P, KANLAYASIRI K. Effects of Ag contents in Sn−*x*Ag lead-free solders on microstructure, corrosion behavior and interfacial reaction with Cu substrate [J]. Transactions of Nonferrous Metals Society of China, 2019, 29(8): 1696−1704.

[20] CHANTARAMANEE S, SUNGKHAPHAITOON P. Influence of bismuth on microstructure, thermal properties, mechanical performance, and interfacial behavior of SAC305−*x*Bi/Cu solder joints [J]. Transactions of Nonferrous Metals Society of China, 2021, 31(5): 1397−1410.

[21] KANLAYASIRI K, KONGCHAYASUKAWAT R. Property alterations of Sn−0.6Cu−0.05Ni−Ge lead-free solder by Ag, Bi, In and Sb addition [J]. Transactions of Nonferrous Metals Society of China, 2018, 28(6): 1166−1175.

[22] WEI Yu-hang, LIU Ying-xia, ZHAO Xiu-chen, TAN Cheng-wen, DONG Ya-ru, ZHANG Ji. Effects of minor alloying with Ge and In on the interfacial microstructure between Zn−Sn solder alloy and Cu substrate [J]. Journal of Alloys and Compounds, 2020, 831: 154−812.

[23] SHALABY R M. Effect of silver and indium addition on mechanical properties and indentation creep behavior of rapidly solidified Bi−Sn based lead-free solder alloys [J]. Materials Science & Engineering A, 2013, 560: 86−95.

[24] NOOR E, ZUHAILAWATI H, RADZALI O. Low temperature In−Bi−Zn solder alloy on copper substrate [J]. Journal of Materials Science: Materials in Electronics, 2016, 8(2): 1−8.

[25] LIU Ying-xia, PU Li, YANG Yong, HE Quan-feng, ZHOU Z, TAN C, ZHAO X, ZHAGN Q, TU K N. A high entropy alloy as very low melting point solder for advanced electronic packaging [J]. Materials Today Advances, 2020, 7: 100101.

[26] ZOU He-fei, ZHANG Qing-ke, ZHANG Zhe-feng. Transition of Bi embrittlement of SnBi/Cu joint couples with reflow temperature [J]. Journal of Materials Research, 2011, 26(3): 449−454.

[27] EI-DAY A A, SWILENM Y, MAKLED M H, EI-SHAARAWY M G, ABDRABOH A M. Thermal and mechanical properties of Sn−Zn−Bi lead-free solder alloys [J]. Journal of Alloys and Compounds, 2009, 484(1/2): 134−142.

[28] SHACKELFORD J F, ALEXANDER W. CRC materials science and engineering handbook [M]. 3rd edition. Chemical Engineering, 2000: 41−41.

[29] ISLAM R A, WU Bo-yi, ALAM M O, CHAN Y C, JILLEK W. Investigations on microhardness of Sn−Zn based lead-free solder alloys as replacement of Sn−Pb solder [J]. Journal of Alloys & Compounds, 2005, 392: 149−158.

[30] SUGANUMA K, MURATA T, NOGUCHI H, TOYODA Y. Heat resistance of Sn−9Zn solder/Cu interface with or without coating [J]. Journal of Materials Research, 2000, 15(4): 884−891.

[31] CHRIAŠTEĽOVÁ J, OŽVOLD M. Properties of solders with low melting point [J]. Journal of Alloys & Compounds, 2008, 457: 323−328.

[32] ZHOU Shi-qi, YANG Chi-han, SHEN Yu-an, LI Shi-kang. The newly developed Sn−Bi−Zn alloy with a low melting point, improved ductility, and high ultimate tensile strength [J]. Materialia, 2019, 6: 10030.

[33] KATTNER U R. Phase diagrams for lead-free solder alloys [J]. The Journal of the Minerals, 2002, 54(12): 45−51.

[34] SUGANUMA K, KIM K S. Sn−Zn low temperature solder [J]. Journal of Materials Science: Materials in Electronics, 2007, 18(1/3): 121−127.

[35] YU Da-quan, XIE Hai-ping, WANG Lai-gui. Investigation of interfacial microstructure and wetting property of newly developed Sn−Zn−Cu solders with Cu substrate [J]. Journal of Alloys & Compounds, 2004, 385: 119−125.

[36] LIU Jian-Chun, ZHANG Gong, WANG Zheng-hong, MA Ju-sheng, SUGANUMA K. Thermal property, wettability and interfacial characterization of novel Sn−Zn−Bi−In alloys as low-temperature lead-free solders [J]. Materials & Design, 2015, 84: 331−339.

[37] ZHOU Jian, SUN Yang-shan, XUE Feng. Properties of low

melting point Sn−Zn−Bi solders [J]. Journal of Alloys and Compounds, 2005, 397(1/2): 260−264.
[38] SONG R W, FLESHMAN C J, WANG Y C, TSAI S Y. IMC suppression and phase stabilization of Cu/Sn−Bi/Cu microbump via Zn doping [J]. Materials Letters, 2021, 282(2): 128735.

$(Sn_{1-x}Zn_x)_{57}(In_{0.78}Bi_{0.22})_{43}$ 低熔点无铅焊料的微观结构表征

张天宇，程 清，竺恒宇，魏琴琴，徐先东

湖南大学 材料科学与工程学院 高分辨电镜中心，长沙 410082

摘 要：为了寻求一种应用于三维集成电路低温焊接的无铅焊料，基于多组元混合的概念设计并表征$(Sn_{1-x}Zn_x)_{57}$-$(In_{0.78}Bi_{0.22})_{43}$ (x=0.10, 0.15, 0.20，摩尔分数，%)四元合金。采用扫描电子显微镜、X 射线衍射仪和差示扫描量热仪研究合金的显微组织、热性能和润湿性。结果表明，合金由金属间化合物 $BiIn_2$、$In_{0.2}Sn_{0.8}$ 和富 Zn 固溶体组成。随着 Zn 添加量的增加，$BiIn_2$ 和富 Zn 相的体积分数增加。合金的熔点低至 70 ℃，源自低熔点金属间化合物 $In_{0.2}Sn_{0.8}$ 和 $BiIn_2$ 的形成；合金具有良好的润湿性，润湿角约为 40°。在合金和 Cu 板的界面结合处形成一种薄而坚韧的 Cu_5Zn_8 层，提高焊点可靠性。研究表明，通过多组元混合概念设计合金可以有效提高焊料的焊接性能。

关键词：无铅焊料；多组元混合；低熔点；显微组织；热性能

(Edited by Bing YANG)